Applied Catalysis B: Environmental 154–155 (2014) 206–212

Contents lists available at ScienceDirect

Applied Catalysis B: Environmental

journal homepage: www.elsevier.com/locate/apcatb

Nitrogen-doped nanodiamond rod array electrode with superior performance for electroreductive debromination of polybrominated diphenyl ethers

Yanming Liu, Shuo Chen, Xie Quan*, Xinfei Fan, Huimin Zhao, Qian Zhao, Hongtao Yu

Key Laboratory of Industrial Ecology and Environment Engineering (Ministry of Education, China), School of Environmental Science and Technology, Dalian University of Technology, Dalian 116024, China

ARTICLE INFO

Article history:
Received 28 April 2013
Received in revised form 10 January 2014
Accepted 13 February 2014
Available online 22 February 2014

Keywords:
Nitrogen-doped nanodiamond
Electrocatalyst
Electroreductive debromination
Polybrominated diphenyl ethers
Diamond rod array.

ABSTRACT

Polybrominated diphenyl ethers (PBDEs) are a class of persistent and toxic pollutants. They are widely distributed in environment and present a potential risk to environment and public health. Thus, it is important to develop effective and feasible methods to remove them from ecosystem. Here, we presented a novel vertically aligned nitrogen-doped nanodiamond (VA-NDD)/Si rod array (RA) electrode with a low hydrogen evolution potential, −1.95 V vs Hg/Hg_2SO_4 electrode, and superior activity for electroreductive debromination of persistent 2,2′,4,4′-tetrabromodiphenyl ether (BDE-47). Over 97% BDE-47 (20 mg/L) was electrochemically reduced in 2 h at −1.85 V with a first-order kinetic constant of 1.93 h^{-1}, which was 8.7 times, 4.7 times, 3.5 times and 2.3 times as great as those of boron-doped diamond (BDD)/Si RA, graphite, Pt wafer and Pd film electrodes under the experimental conditions applied. The durability test demonstrated VA-NDD/Si RA electrode was stable and reusable. Furthermore, the intermediates analysis revealed that BDE-47 could be debrominated completely to diphenyl ether.

1. Introduction

Polybrominated diphenyl ethers (PBDEs), widely used as flame retardants, have attracted wide attention due to their environmental persistence, bioaccumulation, and potential toxicity such as endocrine disruptor, neurotoxicity and developmental toxicity [1,2]. They have been produced in large amounts and are commonly detected in air, water, sediment/soil, biota, and human tissues [3,4]. One of the predominant PBDEs often found in environmental samples is 2,2′,4,4′-tetrabromo diphenyl ether (BDE-47), which has been demonstrated to be more refractory, toxic, water-soluble and bioaccumulative than higher brominated congeners [5–7]. Therefore, development of techniques for decomposing BDE-47 to harmless, biodegradable, or lower toxic species is desirable.

PBDEs are resistant to oxidative treatment due to the strong electron-withdrawing ability originated from their bromine substituents [8]. Current methods for PBDEs removal are mainly focused on reductive debromination, which can convert PBDEs to lower toxic products by the cleavage of C–Br bonds [9]. Meanwhile, biodegradability of the debromination products could be improved compared with PBDEs [10]. The reported debromination methods include biodegradation [11], photolysis [5,6], zerovalent iron or bimetallic nanoparticles reduction [12,13] and electrochemical reduction [14,15]. Among these methods, electrochemical reduction is a promising method owning to its outstanding properties such as debromination without consuming chemical agents, versatility, high energy efficiency, environmental compatibility, and easy handling [14,16,17]. Its degradation efficiency mainly depends on the cathode, which should have high reduction activity, high stability, good conductivity and low hydrogen evolution potential to restrain the side reaction of hydrogen evolution. The reported cathodes with high reduction activity and stability include graphite [18], Pt [19,20], Pd [21,22], Ag [23,24], boron-doped diamond (BDD) [25], N-doped graphene [26] and hybrids based on these active species [27], but PBDEs debromination with these cathodes has suffered from scarcity of noble metals or lack of cathode with low hydrogen evolution potential. Therefore, alternative electrode materials have been actively pursued.

Nanodiamond is a desirable electrode material with excellent chemical stability [28,29]. When N atoms are incorporated in nanodiamond, they can tune its physico-chemical properties, such as electrical conductivity, surface properties and reduction activity [30,31]. The hydrogen evolution potential of N-doped nanodiamond (NDD) electrode will be negatively shifted, much more

* Corresponding author. Tel.: +86 411 84706140; fax: +86 411 84706263.
E-mail address: quanxie@dlut.edu.cn (X. Quan).

http://dx.doi.org/10.1016/j.apcatb.2014.02.028
0926-3373/

negative than that of BDD [32,33]. Moreover, N-doping will introduce uneven charge distribution because the high electronegativity of N polarizes the C–N bonds and the adjacent carbon atoms, and thereby can induce a reduced energy barrier towards electrochemical reactions [34,35]. N-doping can also increase the catalytic sites through inducing strain and defect sites. Based on the above outstanding properties of NDD, it is an attractive material for electrochemical reduction of BDE-47. Among various structures, vertically aligned rod array (VA RA) consisting of nanodiamonds can offer direct channels for effective electron transport and provide a high aspect ratio, leading to improved electrochemical reduction performance [36]. Therefore, VA-NDD/Si RA electrode composed of nanoparticles is designed for the first time in this work, which is expected to provide high electrochemical activity, low hydrogen evolution potential, good conductivity and excellent stability.

In this study, VA-NDD/Si RA electrode was designed for efficient electrochemical reduction of BDE-47. We investigated the effects of nitrogen content and applied potential on electrochemical degradation efficiency. As comparison, the electrochemical reduction experiments were also carried out by the commonly used VA-BDD/Si RA, graphite, Pt wafer and Pd film electrodes.

2. Experimental

2.1. Preparation of VA-NDD/Si RA electrode

The fabrication process of VA-NDD/Si RA electrode is illustrated in Fig. 1. Briefly, a layer of SiO_2 film was grown on the surface of a p-Si (1 1 1) wafer (resistivity 0.05 Ω cm) by thermal oxidation at 900 °C for 2 h. Subsequently, a mask with designed pattern (chromium film with the designed pattern was deposited on the glass plate by sputter; the thickness of chromium film is 100 nm) was coated on the surface of SiO_2 film, and followed by extreme ultraviolet photolithography [37]. Then, the typical Bosch process was employed for etching. SiO_2 film was etched in parallel-plate reactive ion etcher with CF_4 gas (P = 100 W), while Si was etched by inductively coupled plasma with SF_6 gas (coil P = 600 W, platen P = 12 W) and C_4F_8 gas (coil P = 600 W, platen P = 0 W) alternatively. A Si RA substrate was obtained after removing SiO_2 film by HF solution. The surface area for Si RA substrate (2.0 cm × 1.5 cm) is 7.71 cm^2. In order to polish the surface of Si RA substrate and enhance nucleation density during NDD film deposition, Si RA substrate was ultrasonically pre-treated in nanodiamond suspension with acetone as solvent. Then NDD film was deposited on this Si RA substrate by microwave plasma enhanced chemical vapor deposition (MPECVD) at pressure 5.6–6.0 kPa, microwave power 1800 W and a gas mixture of $H_2/CH_4/N_2$ (1% CH_4 in H_2). The flow rate of H_2 was maintained at 99 sccm. The deposition was carried out at 450 °C for 10 h. Three VA-NDD/Si RA electrodes with nitrogen flow rate 1.0 sccm, 1.5 sccm and 2.0 sccm were prepared, which were denoted as VA-NDD1/Si RA, VA-NDD2/Si RA and VA-NDD3/Si RA electrodes, respectively. As a comparison, VA-BDD/Si RA electrode was prepared using the same Si RA substrate and fabrication method with the substitution of N_2 by B_2H_6. The deposition time was 6 h and other growth parameters were same as that reported previously [38].

2.2. Characterizations

The morphology was characterized by scanning electron microscopy (SEM) on a Hitachi S-4800 and transmission electron microscopy (TEM) on an FEI-Tecnai G2 20. Linear sweep voltammetry was conducted on a PARSTAT 2273 electrochemical system (Princeton Applied Research, USA) in a conventional three-electrode cell with VA-NDD/Si RA as the working electrode, a platinum sheet and a Hg/Hg_2SO_4 (saturated K_2SO_4) electrode served as the counter electrode and the reference electrode, respectively. X-ray diffractometer (XRD) pattern was obtained on a Shimadzu LabX XRD-6000 and the Raman spectra were carried out using a Renishaw Micro-Raman system 2000 spectrometer with He–Ne laser excitation (wavelength 623.8 nm). X-ray photoelectron spectroscopy (XPS) was performed with a VG ESCALAB 250 spectrometer using a nonmonochromatized Al Kα X-ray source (1486.6 eV).

2.3. Electrochemical experiments

Electrochemical reduction of BDE-47 was carried out at room temperature with a divided-cell reactor that is schematically shown in Fig. S1. An initial BDE-47 concentration of 20 mg/L (80.0 mL) was used in all of the experiments with 0.05 M H_2SO_4 as supporting electrolyte. The solvent was a mixture of CH_3OH and H_2O with volume ratio 7:3. VA-NDD/Si RA, VA-BDD/Si RA, graphite (20 mm × 30 mm, Haimen Kexing Carbon Co. Ltd.), Pt wafer (20 mm× 30 mm, Tianjin Aida Hengsheng Technology Co. Ltd.) and Pd film electrodes were used as the working electrodes with an effective area of 3.0 cm^2 (preparation of Pd film electrode was described in our previous work [39]). The gap between the working electrode and the counter electrode was about 3.0 cm. The experiments were performed potentiostatically from −1.25 to −2.05 V.

2.4. Analytical methods

During the electrochemical reduction process, BDE-47 samples collected at certain time intervals were analyzed by HPLC (Waters-2695, Waters, U.S.) equipped with a TC-C18 column and ultraviolet detector. The working wavelength was 220 nm and the column oven was set at 30 °C. A mixture of methanol/water (90/10, V/V) was used as mobile phase with the flow rate of 1.0 mL/min. Quantitative determination of degradation intermediates was performed by GC/MS (6890/5973, Agilent, USA) equipped with an electron impact ion source and a DB-5MS column. The temperature of GC column was programmed from 80 °C (hold 1 min) to 265 °C (hold 5 min) at the rate of 12 °C/min. The other experimental conditions were as follows: helium as the carrier gas, injection temperature 275 °C, and source temperature 280 °C. The concentration of Br^- was determined with an ion-chromatograph system (Shimadzu SCL-10ASP, Japan). The system was equipped with a Shimpack IC-A3 column and a CCD-10 AVP detector. The mobile phase was a mixture of Tris:H_3BO_3:p-hydroxybenzoic acid = 0.67:3.09:1.10 (W/V) with a flow rate of 1.0 mL/min. The column oven was set at 40 °C. Debromination ratio (R_{Br}) was then calculated as follows:

$$R_{Br} = \left[C_{Br}/(C_0 \times n)\right] \times 100\%$$

where C_{Br} is the concentration of Br^- (mol/L), C_0 is the initial concentration of BDE-47 solution (mol/L), and n refers to the number of Br atoms contained in the BDE-47 molecule.

3. Results and discussion

3.1. Characterization of VA-NDD/Si RA electrode

The SEM images in Fig. 2a reveal that vertically aligned NDD rod arrays have been successfully fabricated. The NDD film covers the Si RA substrate completely and uniformly, which can be observed from the different morphologies between VA-NDD/Si RA electrode and Si RA substrate (Fig. S2). The high resolution SEM image and TEM image (Fig. 2b and c) show that VA-NDD/Si RA electrode consists of nanocrystalline diamond with particle size about 30–80 nm. Fig. 2d represents a SEM image of VA-BDD/Si

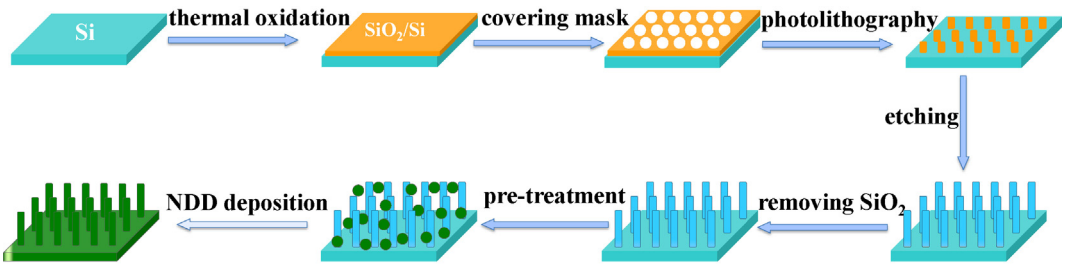

Fig. 1. The procedures for VA-NDD/Si RA electrode preparation.

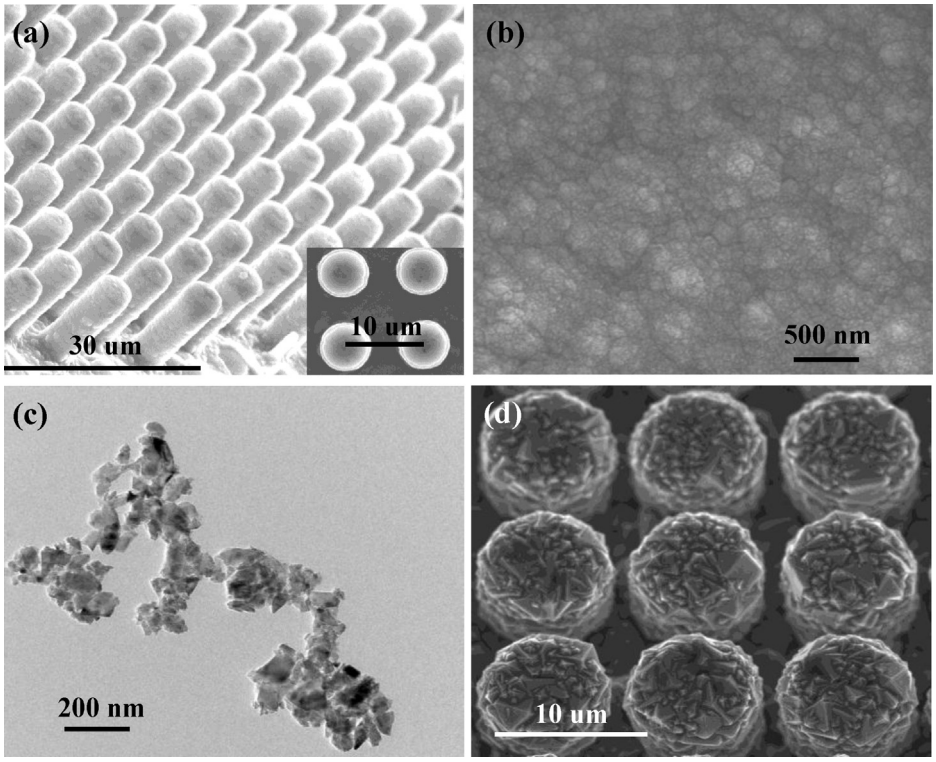

Fig. 2. (a) Side-view SEM image of VA-NDD/Si RA electrode; the inset is the corresponding top-view image; (b) High resolution SEM image of VA-NDD/Si RA electrode; (c) TEM image of VA-NDD/Si RA electrode; (d) Top-view SEM image of VA-BDD/Si RA electrode.

RA electrode deposited under the similar conditions. Although the deposition time of VA-BDD/Si RA electrode is much shorter than that of VA-NDD/Si RA electrode, the particle size of VA-BDD/Si RA electrode is much larger than that of VA-NDD/Si RA electrode. This result indicates that the addition of nitrogen suppresses the diamond growth, leading to the formation of nanocrystalline NDD, which is in accordance with others' works [33].

During the process of electrochemical reduction of pollutants in aqueous solution, most of the energy is consumed by hydrogen evolution reaction if applied potential is more negative than hydrogen evolution potential. Thus, a low hydrogen evolution potential is advantageous for decreasing energy consumed for hydrogen evolution reaction. Here, linear sweep voltammogram was recorded for VA-NDD1/Si RA, VA-NDD2/Si RA, VA-NDD3/Si RA and VA-BDD/Si RA electrodes to evaluate their hydrogen evolution potentials (Fig. 3). The result shows that the hydrogen evolution potential of any of these three VA-NDD/Si RA electrodes is much more negative than that of VA-BDD/Si RA electrode. Among the three VA-NDD/Si RA electrodes, VA-NDD2/Si RA electrode exhibits the lowest hydrogen evolution potential, −1.95 V vs Hg/Hg_2SO_4 electrode. This indicates that VA-NDD2/Si RA electrode is more favorable for enhancing electrochemical degradation efficiency by restraining the hydrogen evolution reaction. Fig. 4 displays the linear sweep

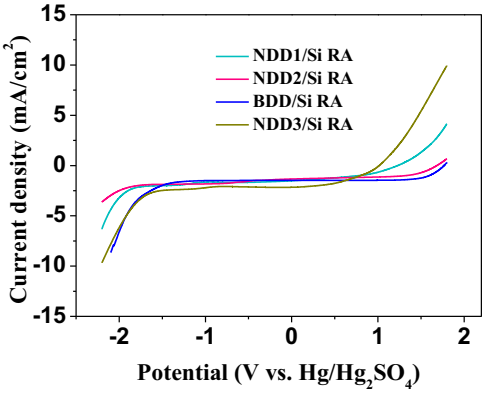

Fig. 3. Linear sweep voltammograms of VA-NDD/Si RA and VA-BDD/Si RA electrodes in 0.05 M H_2SO_4 electrolyte.

voltammogram of VA-NDD2/Si RA electrode in the absence and presence of BDE-47. When the potential is more negative than −0.81 V, current density increases obviously after the addition of BDE-47, indicating the occurrence of BDE-47 reduction on VA-NDD2/Si RA electrode with onset potential −0.81 V. The reduction

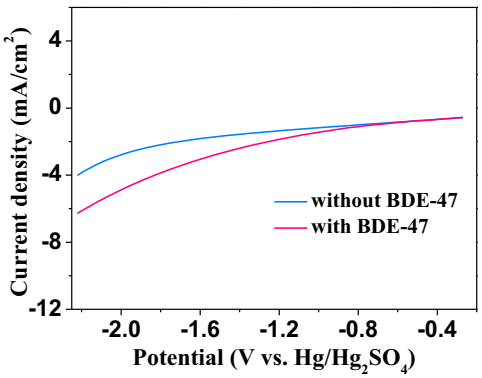

Fig. 4. Linear sweep voltammogram of VA-NDD2/Si RA electrode in the absence and presence of BDE-47 with CH_3OH/H_2O solvent containing 0.05 M H_2SO_4.

peak is not clearly observed from the linear sweep voltammogram, which may be attributed to that the rate-determining step is surface reaction (such as adsorption, desorption) and/or electron transfer.

The XRD pattern of VA-NDD2/Si RA electrode is shown in Fig. 5a. Diffraction peaks at $2\theta = 43.9^\circ$, 75.3° are assigned to (1 1 1) and (2 2 0) planes of cubic diamond, respectively. As shown in Fig. 5b, three peaks at 1168 cm^{-1}, 1332 cm^{-1} and 1560 cm^{-1} can be observed in the Raman spectroscopy. The peak located at 1332 cm^{-1} is the characteristic peak of diamond. The peak around 1168 cm^{-1} is attributed to the presence of *t*-polyacetylene [40,41], which is a polymeric chemical compound formed at the grain boundary of nanocrystalline diamond. The peak at 1560 cm^{-1} arises from the disordered carbon and sp^2 bonded carbon. Successful nitrogen incorporation in diamond is verified by XPS data (Fig. 5c). According to the C 1s spectra, the major component is sp^3 C–C bond (285.6 eV), which is related to the presence of diamond. The sp^2 C–C bond (284.4 eV) reveals the existing of a small quantity of graphitic carbon. The other peaks are related to sp^3 C–N and sp^2 C–N bonds, demonstrating that nitrogen has been doped in diamond. This has been confirmed by the N 1s spectrum of this electrode in Fig. 5d. The peak at 398.6 eV can be assigned to N-sp^3 C bond, while peak at 399.9 eV is ascribed to N-sp^2 C bond. The peak area of N-sp^3 C bond is larger than that of N-sp^2 C bond. It suggests that the nitrogen dopant mainly exists as N-sp^3 C bond. Based on the XPS analysis, the nitrogen content of VA-NDD2/Si RA is 2.26 at% (1.48 at% for VA-NDD1/Si RA and 2.91 at% for VA-NDD3/Si RA).

Table 1
Kinetic constants of BDE-47 degradation under different potentials.

k	−1.25 V	−1.45 V	−1.65 V	−1.85 V	−2.05 V
k_{NDD1} >(h^{-1})	0.36	0.55	0.79	1.16	1.48
k_{NDD2} >(h^{-1})	0.82	1.07	1.5	1.93	2.15
k_{NDD3} >(h^{-1})	0.51	0.81	1.16	1.3	1.42

3.2. Electrochemical reduction of BDE-47

Electrochemical degradation of BDE-47 was carried out to evaluate the reduction activity of VA-NDD/Si RA electrode. We investigated the effects of nitrogen content and applied potential on the electrochemical reduction efficiency; the results are presented in Fig. 6. Over 97% BDE-47 (20 mg/L) is electrochemically reduced by VA-NDD2/Si RA electrode at the first 2 h under applied potential of −1.85 V, which is higher than those by VA-NDD1/Si RA electrode (88.7%) and VA-NDD3/Si RA electrode (92.0%). The difference between their electrochemical degradation rates is more obvious under more positive potential. Electrochemical reduction of BDE-47 follows pseudo-first-order kinetics based on the linear correlation between $\ln(C_0/C_t)$ and t (C_0 is the initial concentration of BDE-47, C_t is the concentration of BDE-47 at time t). According to the kinetic constants (k) of these three electrodes (Table 1), the kinetic constant first increases with increase of nitrogen content under the same applied potential. This suggests that the electrochemical reduction activity of VA-NDD/Si RA electrode is greatly enhanced by increasing nitrogen content. Then the kinetic constant decreases with increase of nitrogen content, which may be ascribed

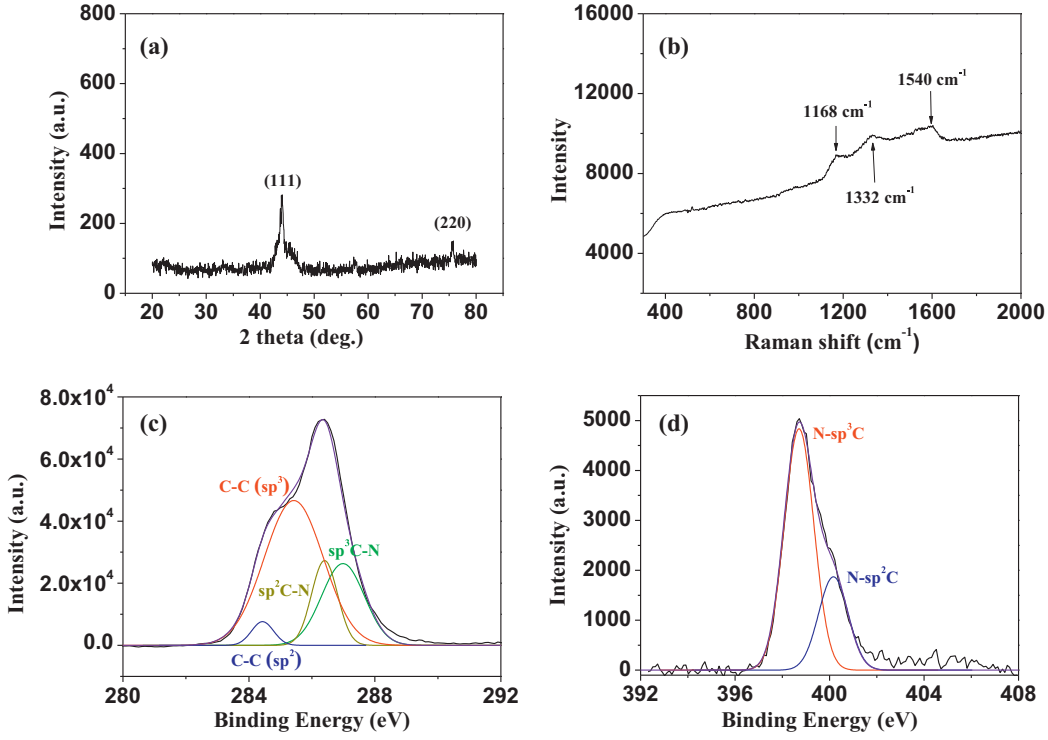

Fig. 5. Physical characterization of VA-NDD2/Si RA electrode: (a) XRD spectra; (b) Raman spectra; (c) C 1s XPS spectra; (d) N 1s XPS spectra.

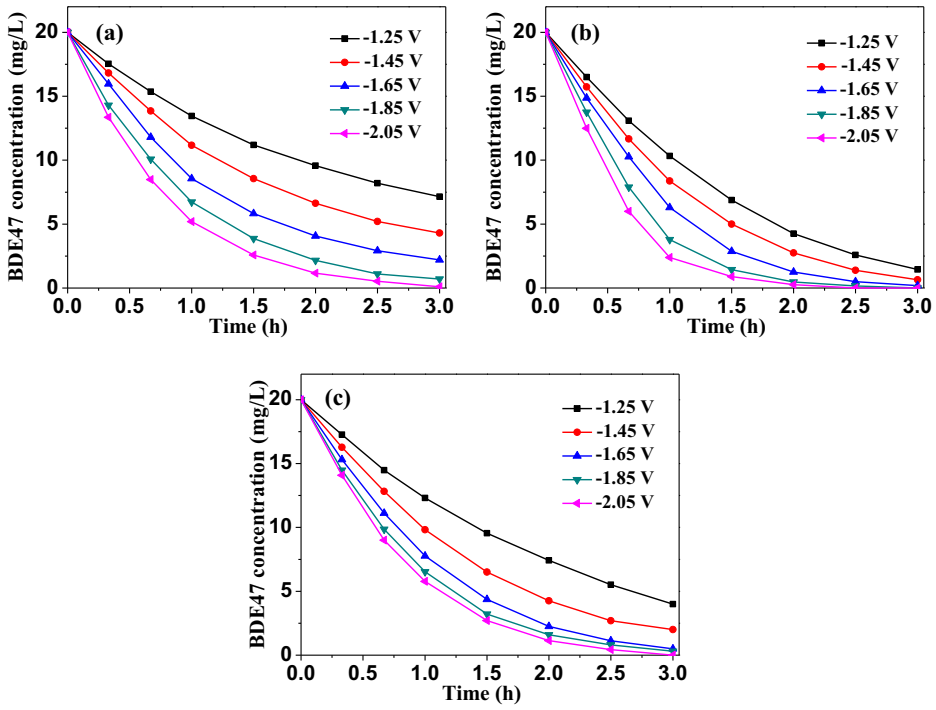

Fig. 6. BDE-47 concentration as a function of time on the (a) VA-NDD1/Si RA electrode; (b) VA-NDD2/Si RA electrode; (c) VA-NDD3/Si RA electrode.

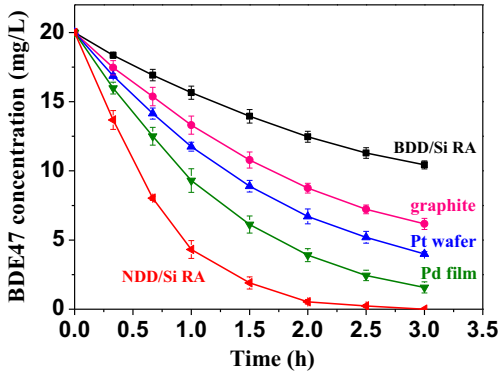

Fig. 7. BDE-47 concentrations as a function of time on different electrodes at potential −1.85 V.

to positively shifted hydrogen evolution potential when nitrogen content is increased to 2%, and then more energy is consumed by hydrogen evolution reaction. The current density related to electrochemical reduction of BDE-47 (defined as effective current density) was obtained by subtracting the current density measured in the presence of BDE-47 from that measured without BDE-47 (Fig. S3). It reveals that the effective current density of VA-NDD2/Si RA electrode is greater than that of VA-NDD3/Si RA electrode, which can explain the decreased kinetic constant of VA-NDD3/Si RA electrode. Therefore VA-NDD2/Si RA electrode is selected for all the following experiments. For VA-NDD2/Si RA electrode, the kinetic constant increases when applied potential is negatively shifted from −1.25 V to −1.85 V. However, the kinetic constant does not increase obviously if the applied potential is further negatively shifted from −1.85 V to −2.05 V.

The electrochemical reduction activity of VA-NDD2/Si RA electrode was compared with other commonly used cathodes (Fig. 7). The first-order kinetic constant (Table 2) of VA-NDD2/Si RA electrode under −1.85 V is 1.93 h^{-1}, which is 8.4 times, 4.7 times, 3.5 times and 2.3 times as great as those of BDD/Si RA, graphite, Pt wafer and Pd film electrodes. Effective current densities of these electrodes were obtained from their linear sweep voltammograms in the absence and presence of BDE-47 (Fig. S4). It reveals the effective current density on VA-NDD2/Si RA is greater than those on VA-BDD/Si RA, graphite, Pt wafer and Pd film electrodes at potential more negative than −1.26 V, which is consistent with the result that kinetic constant of VA-NDD2/Si RA is greater than others' at −1.85 V. The effective current ratios (effective current density to the total current density) of these electrodes for electrochemical reduction of BDE-47 is displayed in Table 2, which suggest that VA-NDD2/Si RA electrode has the highest effective current ratio among these cathodes at −1.85 V. These results demonstrate that NDD has superior electrochemical reduction capability compared with BDD, graphite, or even noble metal electrodes under the experimental conditions applied. Electrochemical reduction of BDE-47 on Ag film (deposited on Si RA substrate according to Ref. [42]) and commercial BDD (Switzerland CSEM Centre) electrodes was also performed for comparison (Fig. S5). It shows that the kinetic constant on VA-NDD2/Si RA electrode is 2.8 times and 11.4 times as great as those on Ag film and commercial BDD electrodes, respectively.

Several important factors may contribute to the excellent electrochemical reduction performance of VA-NDD/Si RA electrode. Firstly, N-doping can increase the catalytic sites through introducing defects [43]. Secondly, hydrogen evolution potential shifts negatively after nitrogen doping, which is also confirmed by others' works reported previously [32,44,45]. In particular, we find that the hydrogen evolution potential is the lowest when nitrogen content is 1.5%. Thirdly, the NDD particles are nano-sized, which can provide an enlarged specific surface area. Moreover, N-doping improves the electrode conductivity, thus enabling facile charge transport.

Table 2
Kinetic constant and steady-state current density of different electrodes.

	NDD2	BDD	Graphite	Pt	Pd
Kinetic constant (h^{-1})	1.93	0.23	0.41	0.55	0.85
Effective current ratio (%)	43.3	14.6	15.5	20.4	25.9

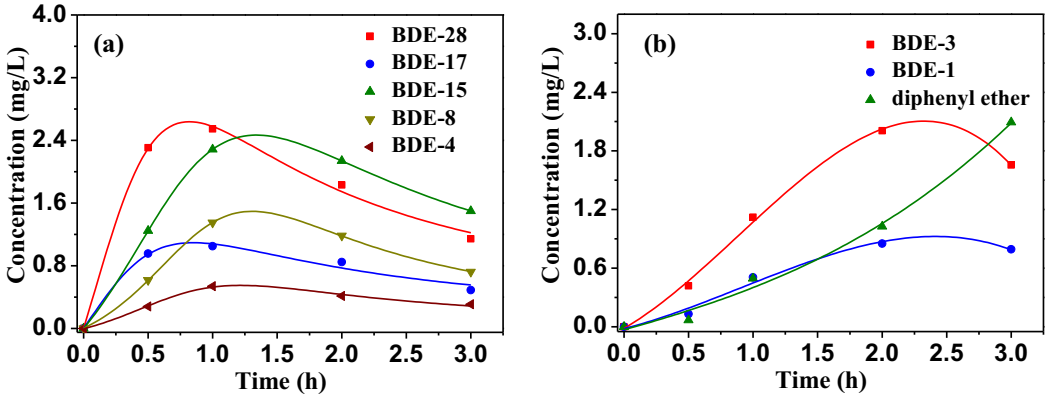

Fig. 8. Concentrations of intermediates as a function of electrolysis time at −1.85 V.

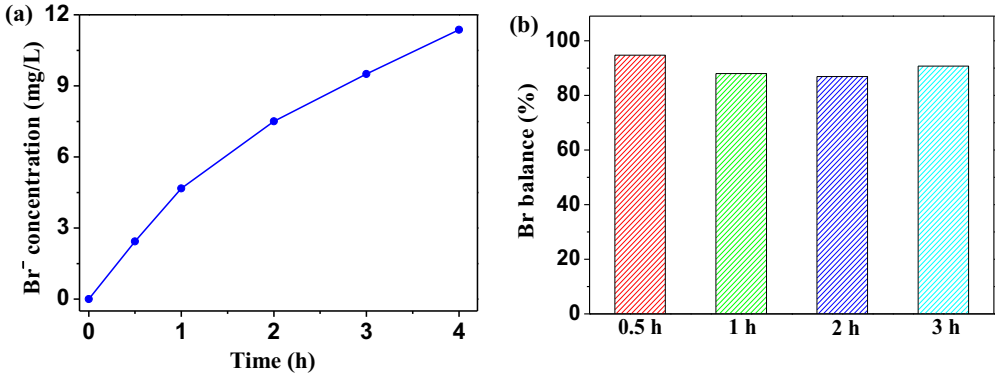

Fig. 9. (a) Br^- concentration as a function of electrolysis time; (b) mass balance of Br for BDE-47 reduction.

The stability of VA-NDD2/Si RA electrode was further investigated by successive electrochemical reduction of BDE-47 for 28 times and the data were recorded every 4 times (Fig. S6). The results reveal that the electrochemical activity of VA-NDD2/Si RA electrode does not decrease during these repeated experiments, which indicates that VA-NDD2/Si RA electrode has great potential for practical application in electrocatalysis for environmental remediation and pollution control.

3.3. Intermediates analysis and degradation mechanism

During electrochemical reduction of BDE-47 by NDD2/Si RA electrode at −1.85 V, the produced intermediates were analyzed by GC/MS. Meanwhile, charges consumed at different times of this electrochemical reduction process are presented at Fig. S7. It shows that the total charge consumed is about 74.2 C. Fig. 8 shows the concentrations of intermediates determined by GC/MS after electrolysis for 30 min, 1 h, 2 h and 3 h. It reveals that BDE-47 is debrominated to their lower brominated intermediates gradually and at last to diphenyl ether. The main products are tri-BDEs and di-BDEs at the first 30 min, including 2,4,4′-tribromodiphenyl ether (BDE-28), 2,2′,4′-tribromodiphenyl ether (BDE-17), and 4,4′-dibromodiphenyl ether (BDE-15). Then the concentrations of tri-BDEs decrease with increase of electrolysis time, leading to the increase of di-BDEs, mono-BDEs and diphenyl ether. The concentrations of di-BDEs increase during the first 1 h but decrease gradually after reaching the maximum, while the concentrations of mono-BDEs (dominated by 4-monobromodiphenyl ether, BDE-3) increase over time at 0–2 h; further electrochemical reduction results in the decrease of mono-BDEs concentration. The completely debromination product, diphenyl ether, is detected after electrolysis for at least 30 min and its concentration increases

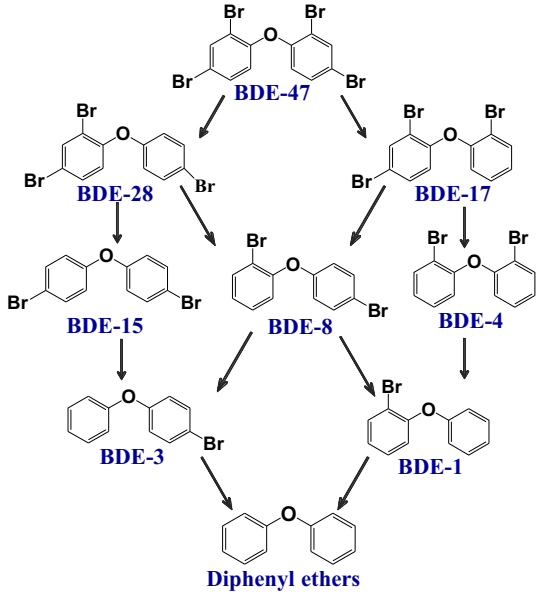

Fig. 10. Simplified debromination pathway of BDE-47.

continuously during the whole electrochemical reduction process. These results indicate that BDE-47 is degraded by NDD2/Si RA electrode through electroreductive debromination.

The Br^- concentration at different electrolysis time is shown in Fig. 9a. It is observed that the Br^- concentration increases with increase of electrolysis time. After electrolysis for 3 h, BDE-47 could not be detected by HPLC, but the Br^- concentration continues

to increase even after the disappearance of BDE-47, indicating the lower brominated intermediates can be further debrominated with longer electrolysis time. When BDE-47 is electrochemically reduced for 4 h, the debromination ratio reaches 86.5% (greater than 75%, the debromination ratio if all BDE-47 is debrominated to mono-BDEs). It suggests that most of BDE-47 is debrominated completely. The mass balance of Br was also investigated in this work. As presented in Fig. 9b, the mass balance of Br ($\{Br_{in\ BDE\text{-}47,undegraded} + Br_{in\ intermediates} + Br^-\}/Br_{in\ BDE\text{-}47,initial}$) shows high recovery rates around 86.7–94.6% at different electrolysis times.

Based on the above results, the possible electroreductive debromination pathway of BDE-47 is proposed as follows (Fig. 10). At first, a bromine atom is substituted by a hydrogen atom through electroreductive debromination by NDD2/Si RA electrode and tri-BDEs (BDE-28, BDE-17) are produced. In the subsequent step, tri-BDEs are debrominated to BDE-15, BDE-8 and BDE-4. These newly formed di-BDEs are further transformed to mono-BDEs (BDE-3 and BDE-1). At last BDE-47 is debrominated completely, and the final product is diphenyl ether.

4. Conclusions

In summary, a novel VA-NDD/Si RA electrode with a low hydrogen evolution potential and high electrochemical reduction activity has been successfully synthesized by MPECVD. This electrode shows excellent performance towards electroreductive debromination of BDE-47. Its kinetic constant is much greater than those of VA-BDD/Si RA, graphite, Pt wafer and Pd film electrodes under the experimental conditions applied. The significant enhancement of its electrochemical reduction performance is attributed to the low hydrogen evolution potential, N-doping induced active sites, enlarged surface area and facile charge transport. Moreover, this electrode is stable and reusable, which is important for practical application. This work indicates NDD can be considered as one of the promising electrocatalytic materials for electrochemical reduction.

Acknowledgments

This work was supported by National Basic Research Program of China (2011CB936002).

Appendix A. Supplementary data

Supplementary data associated with this article can be found, in the online version, at http://dx.doi.org/10.1016/j.apcatb.2014.02.028.

References

[1] P.O. Darnerud, Environ. Int. 29 (2003) 841–853.
[2] P. Eriksson, E. Jakobsson, A. Fredriksson, Environ. Health Perspect. 109 (2001) 903–908.
[3] T. Bhaskar, T. Matsui, M.A. Uddin, J. Kaneko, A. Muto, Y. Sakata, Appl. Catal., B 43 (2003) 229–241.
[4] D.M. Guvenius, A. Aronsson, G. Ekman-Ordeberg, A. Bergman, K. Norén, Environ. Health Perspect. 111 (2003) 1235–1241.
[5] G. Soderstrom, U. Sellstrom, C.A. De Wit, M. Tysklind, Environ. Sci. Technol. 38 (2004) 127–132.
[6] J. Eriksson, N. Green, G. Marsh, A. Bergman, Environ. Sci. Technol. 38 (2004) 3119–3125.
[7] P.O. Darnerud, G.S. Eriksen, T. Johannesson, P.B. Larsen, M. Viluksela, Environ. Health Perspect. 109 (2001) 49–68.
[8] P.M. Bastos, J. Eriksson, J. Vidarson, A. Bergman, Environ. Sci. Pollut. Res. Int. 15 (2008) 606–613.
[9] L.K. Lee, C. Ding, K.L. Yang, J.Z. He, Environ. Sci. Technol. 45 (2011) 8475–8482.
[10] D. Kim, J.R. Chen, T.F. Yen, J. Hazard. Mater. 163 (2009) 231–238.
[11] A.C. Gerecke, P.C. Hartmann, N.V. Heeb, H.P.E. Kohler, W. Giger, P. Schmid, M. Zennegg, M. Kohler, Environ. Sci. Technol. 39 (2005) 1078–1083.
[12] Y.S. Keum, Q.X. Li, Environ. Sci. Technol. 39 (2005) 2280–2286.
[13] Y. Zhuang, S. Ahn, R.G. Luthy, Environ. Sci. Technol. 44 (2010) 8236–8242.
[14] J.Y. Su, N. Lu, J.J. Zhao, H.T. Yu, H. Huang, X.L. Dong, X. Quan, J. Hazard. Mater. 231 (2012) 105–113.
[15] P.M.L. Bonin, P. Edwards, D. Bejan, C.C. Lo, N.J. Bunce, A.D. Konstantinov, Chemosphere 58 (2005) 961–967.
[16] L. Szpyrkowicz, S. Daniele, M. Radaelli, S. Specchia, Appl. Catal., B 66 (2006) 40–45.
[17] C.A. Martínez-Huitle, E. Brillas, Appl. Catal., B 87 (2009) 105–145.
[18] Y.X. Fang, S.R. Al-Abed, Appl. Catal., B 80 (2008) 327–334.
[19] K. Miyoshi, Y. Kamegaya, M. Matsumura, Chemosphere 56 (2004) 187–193.
[20] M.A. Hasnata, M. Saiful Alam, M.H. Mahbub-ul Karim, M.A. Rashed, M. Machida, Appl. Catal., B 63 (2006) 161–167.
[21] A.I. Tsyganok, K. Otsuka, Appl. Catal., B 22 (1999) 15–26.
[22] H. Wang, J.L. Wang, Appl. Catal., B 77 (2007) 58–65.
[23] M.T. Buelow, A.J. Gellman, J. Am. Chem. Soc. 123 (2001) 1440–1448.
[24] C. Durante, A.A. Isse, G. Sandonà, A. Gennaro, Appl. Catal., B 88 (2009) 479–489.
[25] F. Marken, C.A. Paddon, D. Asogan, Electrochem. Commun. 4 (2002) 62–66.
[26] H.B. Wang, T. Maiyalagan, X. Wang, ACS Catal. 2 (2012) 781–794.
[27] A.Z. Li, X. Zhao, Y.N. Hou, H.J. Liu, L.Y. Wu, J.H. Qu, Appl. Catal., B 111 (2012) 628–635.
[28] M. Panizza, G. Cerisola, Appl. Catal., B 75 (2007) 95–101.
[29] V.N. Mochalin, O. Shenderova, D. Ho, Y. Gogotsi, Nat. Nanotechnol. 7 (2012) 11–23.
[30] J. Shalini, K.J. Sankaran, C.L. Dong, C.Y. Lee, N.H. Tai, I.N. Lin, Nanoscale 5 (2013) 1159–1167.
[31] J. Birrell, J.A. Carlisle, O. Auciello, D.M. Gruen, J.M. Gibson, Appl. Phys. Lett. 81 (2002) 2235–2237.
[32] I. Yagi, K. Tsunozaki, A. Fujishima, B. Ohtani, K. Uosaki, J. Electrochem. Soc. 149 (2002) E1–E5.
[33] S. Raina, W.P. Kang, J.L. Davidson, Diamond Relat. Mater. 18 (2009) 574–577.
[34] Y.Y. Shao, J.H. Sui, G.P. Yin, Y.Z. Gao, Appl. Catal., B 79 (2008) 89–99.
[35] S.Y. Wang, E. Iyyamperumal, A. Roy, Y.H. Xue, D.S. Yu, L.M. Dai, Angew. Chem. Int. Ed. 50 (2011) 11756–11760.
[36] D.B. Luo, L.Z. Wu, J.F. Zhi, ACS Nano 3 (2009) 2121–2128.
[37] B.S. Flavel, M.J. Sweetman, C.J. Shearer, J.G. Shapter, N.H. Voelcker, ACS Appl. Mater. Interfaces 3 (2011) 2463–2471.
[38] H.B. Yu, C.J. Ma, X. Quan, S. Chen, H.M. Zhao, Environ. Sci. Technol. 43 (2009) 1935–1939.
[39] C.Y. Cui, X. Quan, H.T. Yu, Y.H. Han, Appl. Catal., B 80 (2008) 122–128.
[40] D. Caschera, B. Cortese, A. Mezzi, M. Brucale, G.M. Ingo, G. Gigli, G. Padeletti, Langmuir 29 (2013) 2775–2783.
[41] T.H. Chang, K. Panda, B.K. Panigrahi, S.C. Lou, C. Chen, H.C. Chan, I.N. Lin, N.H. Tai, J. Phys. Chem. C 116 (2012) 19867–19876.
[42] A.A. Isse, P.R. Mussini, A. Gennaro, J. Phys. Chem. C 113 (2009) 14983–14992.
[43] A. Stacey, D.A. Simpson, T.J. Karle, B.C. Gibson, V.M. Acosta, Z.H. Huang, K.M.C. Fu, C. Santori, R.G. Beausoleil, L.P. McGuinness, K. Ganesan, S. Tomljenovic-Hanic, A.D. Greentree, S. Prawer, Adv. Mater. 24 (2012) 3333–3338.
[44] Y.R. Zhang, S. Yoshihara, T. Shirakashi, T. Kyomen, Diamond Relat. Mater. 14 (2005) 213–219.
[45] L.L.G. Silva, V.J. Trava-Airoldi, E.J. Corat, N. Added, P.T.A. Sumodjo, Diamond Relat. Mater. 16 (2007) 174–180.